

Communication

On-Chip E_{00} – E_{20} Mode Converter Based on Multi-Mode Interferometer

Yuan Zhang¹, Yuexin Yin² , Yingzhi Ding², Shengyuan Zhang¹, Xiaoqiang Sun² , Daming Zhang² 
and Ye Li^{1,*}

¹ School of Physics, Changchun University of Science and Technology, Changchun 130022, China; yuanz@mails.cust.edu.cn (Y.Z.); zhangsy@mails.cust.edu.cn (S.Z.)

² State Key Laboratory of Integrated Optoelectronics, College of Electronic Science and Engineering, Jilin University, Changchun 130012, China; yxyin20@mails.jlu.edu.cn (Y.Y.); dingyz22@mails.jlu.edu.cn (Y.D.); sunxq@jlu.edu.cn (X.S.); zhangdm@jlu.edu.cn (D.Z.)

* Correspondence: liye@cust.edu.cn

Abstract: Mode converters is a key component in mode-division multiplexing (MDM) systems, which plays a key role in signal processing and multi-mode conversion. In this paper, we propose an MMI-based mode converter on 2%- Δ silica PLC platform. The converter transfers E_{00} mode to E_{20} mode with high fabrication tolerance and large bandwidth. The experimental results show that the conversion efficiency can exceed -1.741 dB with the wavelength range of 1500 nm to 1600 nm. The measured conversion efficiency of the mode converter can reach -0.614 dB at 1550 nm. Moreover, the degradation of conversion efficiency is less than 0.713 dB under the deviation of multimode waveguide length and phase shifter width at 1550 nm. The proposed broadband mode converter with high fabrication tolerance is promising for on-chip optical network and commercial applications.

Keywords: integrated optic; mode converter; multimode interference; integrated optics devices



Citation: Zhang, Y.; Yin, Y.; Ding, Y.; Zhang, S.; Sun, X.; Zhang, D.; Li, Y. On-Chip E_{00} – E_{20} Mode Converter Based on Multi-Mode Interferometer. *Micromachines* **2023**, *14*, 1073. <https://doi.org/10.3390/mi14051073>

Academic Editor: Franck Chollet

Received: 20 April 2023

Revised: 11 May 2023

Accepted: 17 May 2023

Published: 18 May 2023



Copyright: © 2023 by the authors. Licensee MDPI, Basel, Switzerland. This article is an open access article distributed under the terms and conditions of the Creative Commons Attribution (CC BY) license (<https://creativecommons.org/licenses/by/4.0/>).

1. Introduction

With the development of new generation communication technology and large-capacity signal processing technology, the demand for high-speed data transmission and large-capacity data processing is increasing. Various multiplexing methods have been proposed for this purpose, such as wavelength division multiplexing (WDM), space division multiplexing (SDM) and polarization division multiplexing (PDM) technologies [1–8]. Mode division multiplexing (MDM) has been considered as a promising technology [9,10] that can significantly improve the capacity of optical communication, on-chip interconnect, and computation [11,12]. Since the orthogonal eigenmodes of the same wavelength propagate in a single channel without inter-channel crosstalk, cooperation with WDM technology, MDM technology increases overall transmission capacity dramatically [13,14]. In MDM system, mode converter with broad bandwidth, low insertion loss, and high mode conversion efficiency is the key components between fundamental mode and higher-order modes at optical nodes [15–20]. Mode converters have been demonstrated on different structures, such as asymmetrical directional couplers (ADCs) [21], Y-branch [22], multi-mode interferometers (MMIs) [23,24]. Although ADCs convertors show low loss and high fabrication tolerant, they suffer from high wavelength dependence. Y-branch convertors contribute high crosstalk between modes. Nowadays, slotted waveguide and etched metasurface waveguide converter show ultra-compact footprint and high efficiency of mode conversion [17,25–28]. However, for commercial usage, large fabrication tolerances, in the micrometer range, are necessary. Compared with other kinds of mode conversion techniques, the mode converters based on MMIs shows broad bandwidth and large fabrication tolerance.

In this paper, we demonstrate an MMI-based mode converter on silica based planar lightwave circuits (PLC) platform with 2% refractive index difference(Δ). The light of E_{00} mode will be converted into E_{20} after propagating through the device. We optimize the mode converter through beam propagation method (BPM). The simulation result shows a conversion efficiency of -0.083 dB at 1550 nm. After fabrication, the converter shows high mode conversion efficiency of -0.614 dB at 1550 nm. From 1500 nm to 1600 nm, the conversion efficiency exceeds -1.741 dB. Moreover, the degradation of conversion efficiency is less than 0.713 dB under the deviation of multimode waveguide length and phase shifter width at 1550 nm. Compared with other mode conversion techniques, our designed MMI-based mode converter reduces the device size while ensuring high conversion efficiency, which has the advantages of broad bandwidth and large fabrication tolerance. The mode converter is suitable for large scale and complex on-chip optical networks. The high fabrication tolerance contributes the devices are promising for commercial application.

2. Design and Simulation

Several material platforms have been investigated for integrated photonics circuits, including silicon-on-insulator (SOI), silicon nitride (SiN), polymer-based PLC and silica-based PLC. SOI and SiN waveguide devices are compact and promising for co-package optics. However, they suffer from low fabrication tolerant and high coupling loss with fiber. Polymer based PLC devices are attractive for thermo-optical switch and high-speed modulators. The stability of polymers is a major limitation to their commercial usage. Compared with other platforms, the silica-based PLC have advantages of low loss, good match of the optical mode field with an optical fiber, and is commercially available. However, the low thermal optical coefficient (TOC) of silica contributes to high power consumption when thermo-optical tuning is used. Therefore, the silica-based PLC platform is suitable for our passive converter.

Figure 1a shows the cross section of single mode waveguide. The thickness is $4\ \mu\text{m}$. With different germanium oxide doping, the refractive index difference between claddings and cores is 2%. Refractive indices are 1.473 and 1.444 at 1550 nm, respectively. According to the calculated relationship between effective refractive indices and waveguide width shown in Figure 1b, we choose $4\ \mu\text{m}$ as the height and width to maintain single mode propagation.

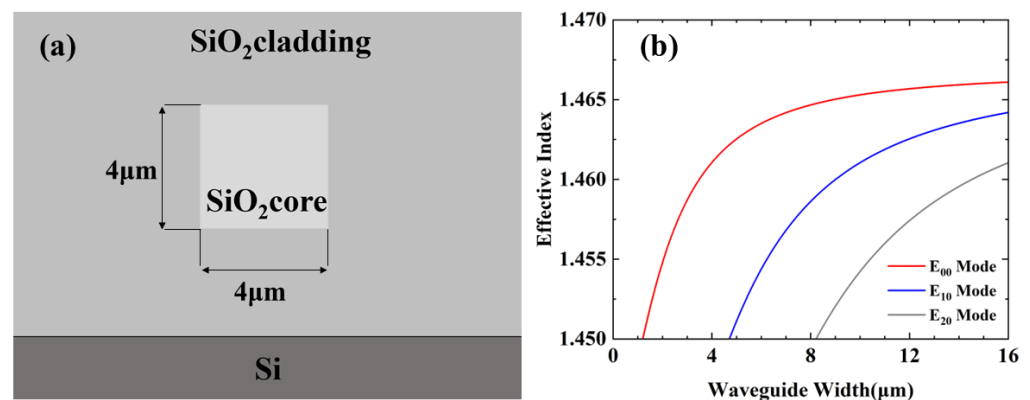


Figure 1. (a) Cross section of the silica waveguide. (b) Calculated effective indices of 4- μm -thickness silica waveguide with different widths.

The schematic of the proposed MMI-based mode converter is demonstrated in Figure 2. The converter is constructed by input waveguide, tapered waveguide, 66% mode converter MMI, phase shifter waveguide, S-bend, and output waveguide. The fundamental mode is coupled into Port 1 (P_{in}) through a tapered waveguide. The 66% E_{00} mode is converted into E_{10} at Port 2 (P_{out}^1) after the first MMI. The light left propagates in fundamental mode through Port 3 (P_{out}^0). A phase shifter is introduced to ensure π phase difference between

E_{00} mode and E_{10} mode. When these lights meet at the second MMI, the mode of light is converted to E_{20} mode at Port 4 (P_{out}).

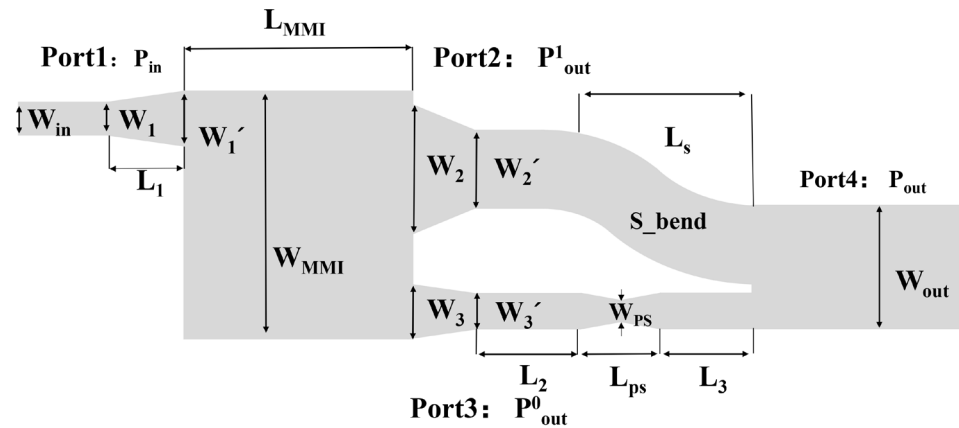


Figure 2. Schematic of the MMI-based mode converter.

The first MMI coupler is a 3×3 MMI with outputs modified into two, one of which is for first-order mode output, another is for fundamental mode output. The length of the conventional 3×3 MMI is equal to the length of the 66% mode converter MMI, which is $L_{MMI} = L_3^1 = 3L_c/3 = L_c$, with L_c as the coupling length based on self-imaging property and it is given by [29]:

$$L_c = \frac{\pi}{\beta_0 - \beta_1} = \frac{4n_r W^2}{3\lambda_0} \tag{1}$$

where β_0 is the fundamental mode propagation constant, β_1 the first-order mode propagation constant, λ_0 is the operation wavelength, n_r is the refractive index of the core waveguide and W is the effective width taking into account the Goos–Hänchen shifts at the ridge boundaries, whose displacement is very small, and can approximately equal to the width of MMI (W_{MMI}). For a conventional 3×3 MMI, when E_{00} mode is input from port P_{in} , the powers at three output ports of E_{00} modes are equal. However, the phases of the three outputs are $\varphi_{11} = \varphi_0 + 5\pi/3$, $\varphi_{12} = \varphi_0 + 2\pi/3$ and $\varphi_{13} = \varphi_0 + \pi$, respectively, where φ_0 is a constant phase. Therefore, the phase difference between the two fundamental modes at Port 2 is π . We combine these two fundamental modes to form E_{10} mode. As for the E_{20} mode, we need a $2/3\pi$ phase shifter. With BPM calculating, the width and length of the phase shifter are $W_{PS} = 3.7 \mu\text{m}$ and $L_{PS} = 200 \mu\text{m}$, respectively.

Based on the above principle, we use BPM for the design and optimization of the device at 1550 nm. To reduce the loss caused by mode mismatch, tapered waveguides are introduced between MMI region and waveguides. Widths of tapers are transferred from $W_1 = 4 \mu\text{m}$, $W_2 = 11.5 \mu\text{m}$ and $W_3 = 4.5 \mu\text{m}$ to $W'_1 = 4.5 \mu\text{m}$, $W'_2 = 10.4 \mu\text{m}$, and $W'_3 = 4 \mu\text{m}$, linearly. The gap between E_{10} mode port and E_{00} mode port is $4.85 \mu\text{m}$. The length of these three tapered waveguides is $35 \mu\text{m}$. There are $100\text{-}\mu\text{m}$ -length straight waveguides after E_{00} and E_{10} mode port. We use S-bend to connect Port 2 with output width. The arc radius of the S-bend is above 2 cm. The loss caused by S-bend could be neglected. The length of the straight waveguide that connects phase shifter and output waveguide is chosen to be $400 \mu\text{m}$. The width of the output waveguide is set to be $15.9 \mu\text{m}$. In our design, the width of the MMI (W_{MMI}) is designed to be $22.25 \mu\text{m}$, which is used to avoid coupling between E_{10} mode and E_{00} mode at ports 2 and 3. Therefore, the calculated MMI coupler length is optimized to be $L_{MMI} = 730 \mu\text{m}$. The length of the output waveguide is $800 \mu\text{m}$. The total length of the mode converter is $2400 \mu\text{m}$.

Figure 3a shows the field distribution of the device at 1550 nm wavelength with fundamental mode is input. Figure 3b shows the fundamental mode field distribution of the input. The mode distributions of E_{10} at port 2 and E_{00} at port 3 of the mode converter MMI are shown in Figure 3c. Figure 3d shows the mode distribution of E_{20} . From Figure 3a, the E_{00} mode is successfully converted to the E_{20} mode. In the simulation, we set the

E_{00} mode input power of port1 to 1 and simulated the conversion efficiency of the mode converter from 1500 nm to 1600 nm, as shown in Figure 3e. The conversion efficiency in percent (E_p) and dB (E_d) are calculated by Equations (2) and (3), respectively. Here, b is the propagation loss of the E_{00} mode in the dB scale [30].

$$E_p = (1 - 10^{0.1b}) \times 100\% \quad (2)$$

$$E_d = 10\lg(1 - 10^{0.1b}) \quad (3)$$

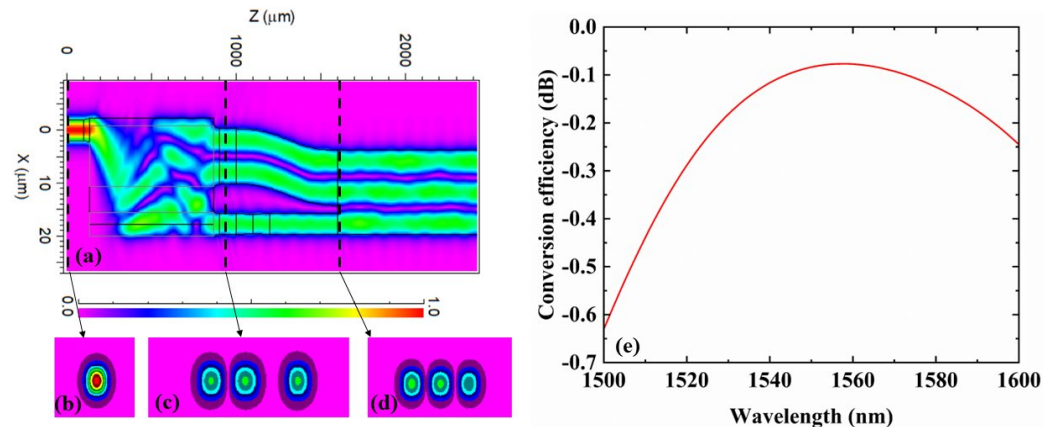


Figure 3. (a) Simulated optical field propagation distribution of the device at 1550 nm. (b) Mode profile of E_{00} at port 1. (c) Mode profile of E_{10} at port 2 and E_{00} at port3. (d) Mode profile of E_{20} at port 4. (e) Simulated conversion efficiency of the mode converter at 1500 nm to 1600 nm.

At 1550 nm wavelength, the conversion efficiency is 96.2% (-0.083 dB). From 1500 nm to 1600 nm, simulation results show that the conversion efficiency exceeds -0.630 dB. In summary, we obtain a mode conversion from E_{00} to E_{20} at 1550 nm with a conversion efficiency of -0.083 dB.

3. Characterization and Discussion

The proposed mode converter was fabricated by the PLC foundry, SHIJIA, China. First, the bottom cladding of ~ 15 μm was thermally oxidized on silicon substrate. Second, we grew a 4 - μm -thickness silica core layer above the bottom cladding by plasma enhanced chemical vapor deposition (PECVD). The waveguide was formed by etching through inductively coupled plasma etching (ICP) technique. Finally, PECVD was again used to deposit the upper cladding. Since the existing coupling test system is difficult to directly monitor the high-order mode power, a mode demultiplexer was introduced at the end of the output waveguide to convert the E_{20} mode to the E_{00} mode to indirectly characterize the higher-order mode power. The mode multiplexer/demultiplexer of E_{20} mode and a reference waveguide are fabricated simultaneously. The microscope images of the demonstrated converter are shown in Figure 4a–d.

In Figure 4a, the measured width of the MMI is 22 μm . The widths of the two output ports are measured in Figure 4b at 10 μm and 4 μm , respectively. The S bend is separated from the phase shifter by a large distance of 5 μm , which can be observed in Figure 4c. The width of the output waveguide is measured to be 16 μm in Figure 4d.

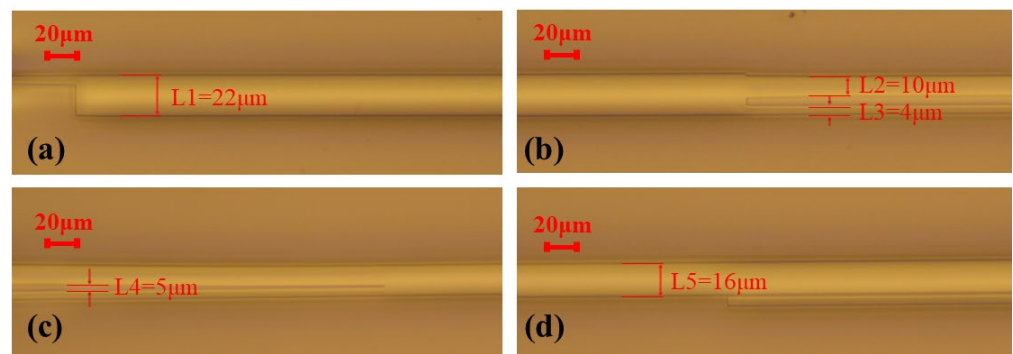


Figure 4. (a–d) Microscopic images of the fabricated mode converter.

The E_{00} mode is coupled into the device by edge coupling system. The spectra of the reference straight waveguide and the mode multiplexed/demultiplexer for the E_{20} mode are shown in Figure 5a. The normalized spectral response of the E_{00} to E_{20} mode converter experimental measure data is shown in Figure 5b. The experimental results show that the conversion efficiency can exceed -1.741 dB with the wavelength range of 1500 nm to 1600 nm. The conversion efficiency of the device is -0.614 dB (87%) at 1550 nm. The maximum conversion efficiency is -0.549 dB (88%) at 1556 nm. The 1-dB bandwidth of the device is 90 nm. The captured output mode patterns at different wavelengths shown in Figure 5c–e.

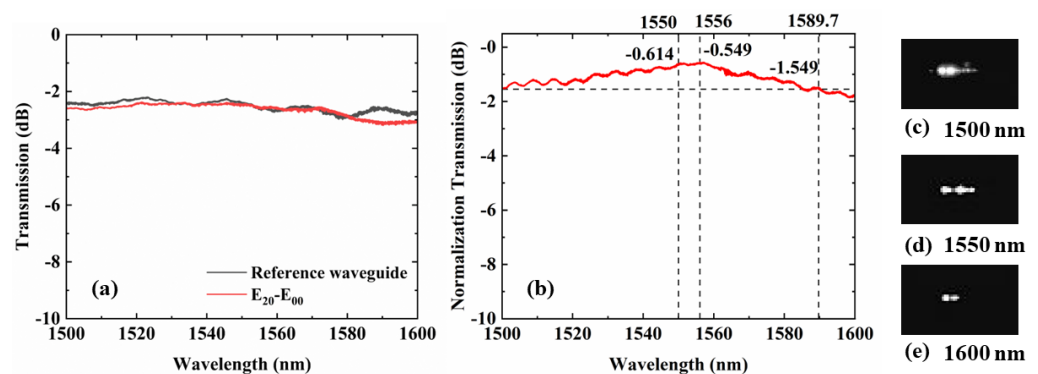


Figure 5. (a) Measured power loss of the reference waveguide with the E_{20} mode (de) multiplexer. (b) Conversion efficiency of the mode converter from E_{00} to E_{20} in the wavelength range from 1500 nm to 1600 nm. Output mode taken from output port at (c) 1500 nm, (d) 1550 nm and (e) 1600 nm.

We fabricate proposed device with different lengths of MMI and widths of phase shifter to perform fabrication tolerant. The key components, MMIs and phase shifters, influence the conversion efficiency of the device a lot. We study the fabrication tolerance by changing length and width of MMI and phase shifter, and observe the output power of E_{20} . The deviations are 0 and ± 10 μm for L_{MMI} and 0 and ± 0.2 μm for W_{PS} . The simulation result is shown in the Figure 6. We can see that when L_{MMI} move away from their optimal values, the conversion efficiency of E_{00} - E_{20} has different degrees of degradation at wavelength 1550 nm., which means that the change of L_{MMI} will cause an impact on the conversion efficiency of the device. At 1550 nm, the conversion efficiency varies from -0.083 dB to -0.234 dB.

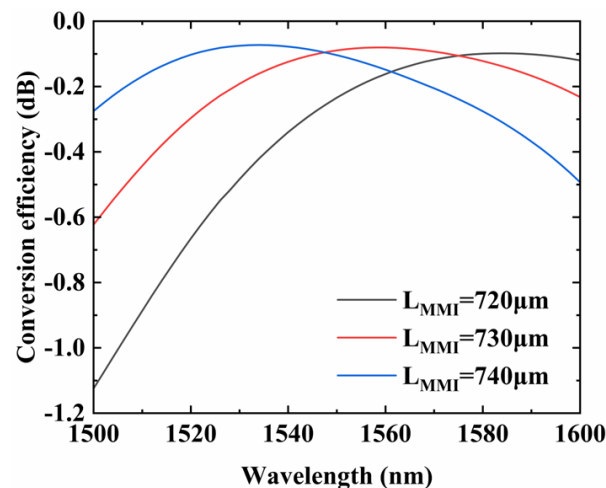


Figure 6. Simulated conversion efficiency of the mode converter when changing the L_{MMI} from 1500 nm to 1600 nm.

Similarly, the influence of W_{PS} on the conversion efficiency of the device is simulated. Figure 7 shows the dependence of the E_{00} – E_{20} conversion efficiency on the W_{PS} . We use the optimal value $L_{MMI} = 730 \mu\text{m}$ as the length of MMI. It can be seen that the change of W_{PS} does have a certain impact on the conversion efficiency of the mode converter. At the wavelength of 1550 nm, the conversion efficiency of the mode converter varies from -0.083 dB to -0.155 dB . Compared with L_{MMI} , the device is more sensitive to W_{PS} .

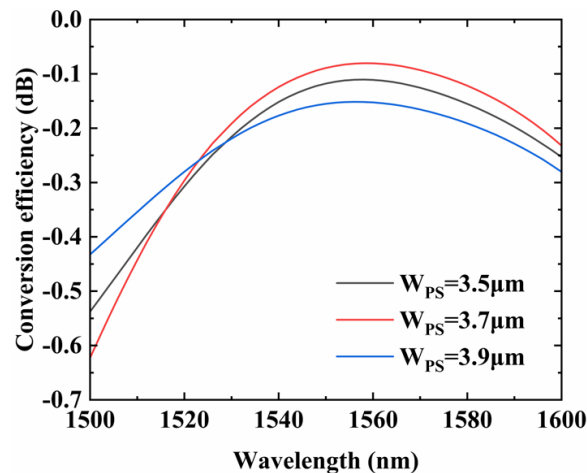


Figure 7. Simulated conversion efficiency of the mode converter when changing the W_{PS} from 1500 nm to 1600 nm.

We summary the spectra of all samples and separate in four groups, as shown in Figure 8a–d. It can be seen that at the wavelength of 1550 nm, the conversion efficiency degradation of the device is less than 0.713 dB when changing L_{MMI} and W_{PS} . However, the conversion efficiency of the converter proposed is lower than others. So there are still some cases that need to be discussed for the MMI-based mode converter we designed. First of all, during the simulation, we initially expected the conversion efficiency to be -0.083 dB (97%) at 1550 nm. However, the actual test results show that the conversion efficiency of the mode converter can only reach -0.614 dB (87%) at 1550 nm. The reason is the differences in geometry and refractive index of cores with respect to design parameters. The device has good repeatability, parameter scanning will help but only if you also have good repeatability. This problem is solved by parameter scanning while fabrication. Secondly, in Figure 8a,d, we note that when $L_{MMI} = 720 \mu\text{m}$ the normalized transmission may exceed 0, which is caused by the normalization procedure owing to the vibration of the reference waveguide.

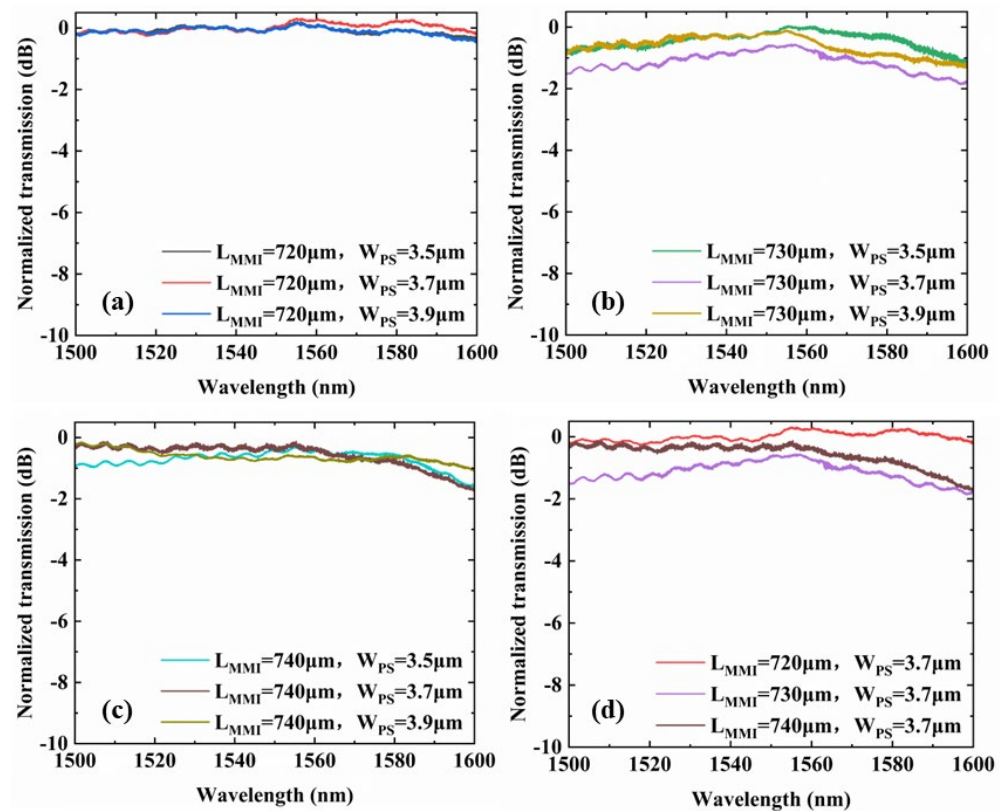


Figure 8. (a–c) The effect of W_{PS} on the conversion efficiency of the mode converter at a given fabrication error range for wavelengths ranging from 1550 nm to 1600 nm with L_{MMI} of 720 μm , 730 μm and 740 μm , respectively. (d) The effect of L_{MMI} on the conversion efficiency of the mode converter at a given fabrication error range for wavelengths ranging from 1550 nm to 1600 nm when W_{PS} is fixed to 3.7 μm .

4. Discussion

In order to clearly demonstrate the mode converter, Table 1 illustrates the performance comparisons between the reported E_{00} – E_{20} mode converters. The compact silicon-on-insulator based device using a 1×4 Y-junction and 4×4 MMI couplers can realize 16 different input-output mode conversions in C-band [31]. The mode converter with a cascaded tapers structure exhibits balanced performances [32]. The mode converter designed in Ref. [33] with phase change material inlaid in multimode waveguide has a large bandwidth and high conversion efficiency. However, the mode converters in these reports only have simulation results and are not actually fabricated. Owing to the low fabrication tolerance of the SOI platform, the device is hard to fabricate with the designed characteristics. Moreover, the SOI device is fixed after fabrication. To obtain a flexible and reconfigurable device, mode switching is necessary for the MDM system. The mode switch based on phase change materials or van der Waals materials can be used to achieve low power consumption and higher-order reconfigurable mode conversion [33–35]. In ref. [36], a mode converter based on cascaded long-period waveguide grating is mentioned, which uses the UV-curable polymer material EPO as the design material. The conversion efficiency of the device can be estimated to be more than 90% at 1550 nm. The polymer-based PLC is a low-cost platform. The design method could be verified on polymer. The design method is also inspiring for silica-based PLC. After comparison, the device proposed shows high conversion efficiency, high tolerance and large bandwidth, which has a good application prospect in MDM system.

Table 1. Comparison the designed E_{00} – E_{20} mode converter with reported works.

Refs.	S/E	BW (nm)	CE (%)	Structure	Materials	Footprint (μm^2)
[29]	E	35	93	MMI+ phase shifter	SOI	1230×8
[31]	S	35	98	Y-junction + MMI	SOI	288×6.8
[32]	S	100	93	Cascaded tapers	SOI	2.5×6.5
[33]	S	245	99	PCM inlaid in multimode waveguide	SOI	2.3×1.82
[34]	E	At 1550 nm	90	Long-period gratings	Polymer PLC	/
This work	E	90	87	MMI + phase shifter	Silica PLC	2400×22.25

S/E, Simulation/Experiment; BW, Bandwidth; CE, Conversion efficiency; PCM, Phase change material; /, Not mentioned.

5. Conclusions

In this work, we proposed an MMI-based mode converter that has the capability to efficiently convert E_{00} mode to E_{20} mode. The experimental results show that the fabricated device has high tolerance and high conversion efficiency, and the efficiency of the fabricated mode converter is -0.614 dB at 1550 nm wavelength. The degradation of conversion efficiency is less than 0.713 dB within the range of fabricate deviation. This paper provides a solution for efficient conversion in MDM systems.

Author Contributions: Conceptualization, Y.Z., Y.Y., D.Z.; methodology, Y.Z., Y.D., D.Z. and Y.L.; investigation, Y.Z., Y.D. and S.Z.; writing—original draft preparation, Y.Z., Y.Y. and Y.D.; writing—review and editing, all authors; supervision, D.Z., X.S. and Y.L.; project administration, D.Z., X.S. and Y.L. All authors have read and agreed to the published version of the manuscript.

Funding: This work is supported by the National Key Research and Development (R&D) Program of China, NO. 2021YFB2800202.

Data Availability Statement: Not applicable.

Conflicts of Interest: The authors declare no conflict of interest.

References

- Winter, M.; Setti, D.; Petermann, K. Cross-Polarization Modulation in Polarization-Division Multiplex Transmission. *IEEE Photonics Technol. Lett.* **2010**, *22*, 538–540. [[CrossRef](#)]
- Chun, H.; Rajbhandari, S.; Faulkner, G.; Tsonev, D.; Xie, E.; McKendry, J.J.D.; Gu, E.; Dawson, M.D.; O'Brien, D.C.; Haas, H. LED Based Wavelength Division Multiplexed 10 Gb/s Visible Light Communications. *J. Light. Technol.* **2016**, *34*, 3047–3052. [[CrossRef](#)]
- Mizuno, T.; Takara, H.; Sano, A.; Miyamoto, Y. Dense Space-Division Multiplexed Transmission Systems Using Multi-Core and Multi-Mode Fiber. *J. Light. Technol.* **2016**, *34*, 582–592. [[CrossRef](#)]
- Goossens, J.W.; Yousefi, M.I.; Jaouen, Y.; Hafermann, H. Polarization-division multiplexing based on the nonlinear Fourier transform. *Opt. Express* **2017**, *25*, 26437–26452. [[CrossRef](#)]
- Zhang, Y.; Pan, S. Photonics-based multi-function analog signal processor based on a polarization division multiplexing Mach-Zehnder modulator. *Opt. Lett.* **2017**, *42*, 5034–5037. [[CrossRef](#)]
- Gao, Y.; Xu, Y.; Ji, L.; Sun, X.; Wang, F.; Wang, X.; Wu, Y.; Zhang, D. Scalable compact mode (de)multiplexer based on asymmetric Y-junctions. *Opt. Commun.* **2019**, *438*, 34–38. [[CrossRef](#)]
- Han, X.; Xiao, H.; Liu, Z.; Zhao, T.; Jia, H.; Yang, J.; Eggleton, B.J.; Tian, Y. Reconfigurable On-Chip Mode Exchange for Mode-Division Multiplexing Optical Networks. *J. Light. Technol.* **2019**, *37*, 1008–1013. [[CrossRef](#)]
- Yang, Y.; Liu, J.; Cheng, R.; Jia, J.; Gao, Y.; Shen, L.; Chen, Z.; He, Y.; Li, J. SDM-WDM ROADM Based on Direct-Laser-Writing SDM Core Separator. *IEEE Photonics J.* **2022**, *14*, 7230506. [[CrossRef](#)]
- Memon, A.K.; Chen, K.X. Recent advances in mode converters for a mode division multiplex transmission system. *Opto-Electron. Rev.* **2023**, *29*, 13–32. [[CrossRef](#)]
- Sun, S.; Che, Y.; Zhu, M.; Lian, T.; Sun, X.; Wang, X.; Huang, Q.; Zhang, D. Mode-insensitive 3-dB power splitter based on multimode-interference coupler. *Opt. Laser Technol.* **2023**, *159*, 109017. [[CrossRef](#)]
- Ye, M.; Yu, Y.; Sun, C.; Zhang, X. On-chip data exchange for mode division multiplexed signals. *Opt. Express* **2016**, *24*, 528–535. [[CrossRef](#)]

12. Gao, Y.; Zhang, D.; Xu, Y.; Fan, X.; Wang, F.; Sun, X. Ultra-broadband polymer E00/E10 mode converter. *Opt. Commun.* **2022**, *508*, 127715. [[CrossRef](#)]
13. Yu, Y.; Ye, M.; Fu, S. On-Chip Polarization Controlled Mode Converter with Capability of WDM Operation. *IEEE Photonics Technol. Lett.* **2015**, *27*, 1957–1960. [[CrossRef](#)]
14. Luo, L.W.; Ophir, N.; Chen, C.P.; Gabrielli, L.H.; Poitras, C.B.; Bergmen, K.; Lipson, M. WDM-compatible mode-division multiplexing on a silicon chip. *Nat. Commun.* **2014**, *5*, 3069. [[CrossRef](#)]
15. Frandsen, L.H.; Elesin, Y.; Frelsen, L.F.; Mitrovic, M.; Ding, Y.; Sigmund, O.; Yvind, K. Topology optimized mode conversion in a photonic crystal waveguide fabricated in silicon-on-insulator material. *Opt. Express* **2014**, *22*, 8525–8532. [[CrossRef](#)]
16. Deng, Q.; Yan, Q.; Liu, L.; Li, X.; Michel, J.; Zhou, Z. Robust polarization-insensitive strip-slot waveguide mode converter based on symmetric multimode interference. *Opt. Express* **2016**, *24*, 7347–7355. [[CrossRef](#)]
17. Ye, W.; Yuan, X.; Gao, Y.; Liu, J. Design of broadband silicon-waveguide mode-order converter and polarization rotator with small footprints. *Opt. Express* **2017**, *25*, 33176–33183. [[CrossRef](#)]
18. Wang, H.; Zhang, Y.; He, Y.; Zhu, Q.; Sun, L.; Su, Y. Compact Silicon Waveguide Mode Converter Employing Dielectric Metasurface Structure. *Adv. Opt. Mater.* **2018**, *7*, 1801191. [[CrossRef](#)]
19. Chen, R.; Bai, B.; Yang, F.; Zhou, Z. Ultra-compact hybrid plasmonic mode converter based on unidirectional eigenmode expansion. *Opt. Lett.* **2020**, *45*, 803–806. [[CrossRef](#)]
20. Wang, T.; Guo, H.; Chen, H.; Yang, J.; Jia, H. Ultra-compact reflective mode converter based on a silicon subwavelength structure. *Appl. Opt.* **2020**, *59*, 2754–2758. [[CrossRef](#)]
21. Sun, Y.; Xiong, Y.; Ye, W.N. Experimental demonstration of a two-mode (de)multiplexer based on a taper-etched directional coupler. *Opt. Lett.* **2016**, *41*, 3743–3746. [[CrossRef](#)] [[PubMed](#)]
22. Driscoll, J.B.; Grote, R.R.; Souhan, B.; Dadap, J.I.; Lu, M.; Osgood, R.M. Asymmetric Y junctions in silicon waveguides for on-chip mode-division multiplexing. *Opt. Lett.* **2013**, *38*, 1854–1856. [[CrossRef](#)] [[PubMed](#)]
23. Gao, Y.; Sun, X.; Li, P.; Zhang, D. Polymer Mode Selecting Switch Based on Cascaded MMI Couplers. *IEEE Photonics Technol. Lett.* **2021**, *33*, 147–150. [[CrossRef](#)]
24. Ou, X.; Yang, Y.; Tang, B.; Li, D.; Sun, F.; Zhang, P.; Liu, R.; Li, B.; Li, Z. Low-loss silicon nitride strip-slot mode converter based on MMI. *Opt. Express* **2021**, *29*, 19049–19057. [[CrossRef](#)]
25. Li, Z.; Kim, M.H.; Wang, C.; Han, Z.; Shrestha, S.; Overvig, A.C.; Lu, M.; Stein, A.; Agarwal, A.M.; Loncar, M.; et al. Controlling propagation and coupling of waveguide modes using phase-gradient metasurfaces. *Nat. Nanotechnol.* **2017**, *12*, 675–683. [[CrossRef](#)]
26. Meng, Y.; Liu, Z.; Xie, Z.; Wang, R.; Qi, T.; Hu, F.; Kim, H.; Xiao, Q.; Fu, X.; Wu, Q.; et al. Versatile on-chip light coupling and (de)multiplexing from arbitrary polarizations to controlled waveguide modes using an integrated dielectric metasurface. *Photonics Res.* **2020**, *8*, 564–576. [[CrossRef](#)]
27. Zhao, Y.; Guo, X.; Zhang, Y.; Xiang, J.; Wang, K.; Wang, H.; Su, Y. Ultra-compact silicon mode-order converters based on dielectric slots. *Opt. Lett.* **2020**, *45*, 3797–3800. [[CrossRef](#)]
28. Meng, Y.; Chen, Y.; Lu, L.; Ding, Y.; Cusano, A.; Fan, J.A.; Hu, Q.; Wang, K.; Xie, Z.; Liu, Z.; et al. Optical meta-waveguides for integrated photonics and beyond. *Light Sci. Appl.* **2021**, *10*, 235. [[CrossRef](#)]
29. Jifang, Q.; Daolin, Z.; Ye, T.; Jian, W.; Yan, L.; Yue, W. Performance Analysis of a Broadband Second-Order Mode Converter Based on Multimode Interference Coupler and Phase shifter. *IEEE Photonics J.* **2015**, *7*, 1–8. [[CrossRef](#)]
30. Xu, Y.; Gao, Y.; Liu, S.; Liu, T.; Sun, X.; Tang, B.; Zhang, P.; Zhang, D. Wideband E00-E10 Silicon Mode Converter Based on 180 nm CMOS Technology. *Appl. Sci.* **2022**, *12*, 10688. [[CrossRef](#)]
31. Linh, H.D.T.; Dung, T.C.; Tanizawa, K.; Thang, D.D.; Hung, N.T. Arbitrary TE₀/TE₁/TE₂/TE₃ Mode Converter Using 1 × 4 Y-Junction and 4 × 4 MMI Couplers. *IEEE J. Sel. Top. Quantum Electron.* **2020**, *26*, 1–8. [[CrossRef](#)]
32. Chen, Z.; Lin, T.; Liu, X.; Lv, H. Ultra-Compact Broadband In-Line Mode Converter Based on a Width-Modulated Silicon Waveguide. *IEEE Photonics J.* **2021**, *13*, 1–7. [[CrossRef](#)]
33. Fei, Y.; Xu, Y.; Huang, D.; Dong, Y.; Zhang, B.; Ni, Y.; Wai, P.K.A. On-Chip Reconfigurable and Ultracompact Silicon Waveguide Mode Converters Based on Nonvolatile Optical Phase Change Materials. *Nanomaterials* **2022**, *12*, 4225. [[CrossRef](#)]
34. Wuttig, M.; Bhaskaran, H.; Taubner, T. Phase-change materials for non-volatile photonic applications. *Nat. Photonics* **2017**, *11*, 465–476. [[CrossRef](#)]
35. Meng, Y.; Feng, J.; Han, S.; Xu, Z.; Mao, W.; Zhang, T.; Kim, J.S.; Roh, I.; Zhao, Y.; Kim, D.-H.; et al. Photonic van der Waals integration from 2D materials to 3D nanomembranes. *Nat. Rev. Mater.* **2023**. [[CrossRef](#)]
36. Jin, W.; Chiang, K.S. Mode converters based on cascaded long-period waveguide gratings. *Opt. Lett.* **2016**, *41*, 3130–3133. [[CrossRef](#)]

Disclaimer/Publisher’s Note: The statements, opinions and data contained in all publications are solely those of the individual author(s) and contributor(s) and not of MDPI and/or the editor(s). MDPI and/or the editor(s) disclaim responsibility for any injury to people or property resulting from any ideas, methods, instructions or products referred to in the content.